THE JOURNAL OF BIOLOGICAL CHEMISTRY VOL. 287, NO. 8, pp. 5554–5561, February 17, 2012


# Fluorescent Recovery after Photobleaching (FRAP) Analysis of Nuclear Export Rates Identifies Intrinsic Features of Nucleocytoplasmic Transport*[S]

Received for publication, September 15, 2011, and in revised form, December 13, 2011 Published, JBC Papers in Press, December 21, 2011, DOI 10.1074/jbc.M111.304899

**Francesco Cardarelli**[‡1], **Luca Tosti**[§1], **Michela Serresi**[‡2], **Fabio Beltram**[‡§], **and Ranieri Bizzarri**[‡§3]

*From the* [‡]*Center for Nanotechnology Innovation @ NEST, Istituto Italiano di Tecnologia, Piazza San Silvestro 12-56127 Pisa, Italy and the* [§]*NEST, Scuola Normale Superiore and Istituto Nanoscienze-CNR, Piazza San Silvestro 12-56127 Pisa, Italy*

**Background:** A dedicated cell machinery oversees energy-dependent nucleocytoplasmic translocation of most proteins.
**Results:** The Fluorescent Recovery after Photobleaching technique reveals high similarity between export and import fluxes, which are nonetheless uncoupled.
**Conclusion:** Our results suggest differential gating properties at individual nuclear pore level.
**Significance:** Our findings can help clarify the mechanism governing energy-dependent translocation through nuclear pores.

**A quantitative description of carrier-mediated nuclear export in live cells is presented. To this end, we fused a prototypical leucine-rich nuclear export signal (NES) to GFP as a cargo model and expressed the fluorescent chimera in live CHO-K1 cells. By modeling FRAP data, we calculate the NES affinity for the export machinery and the maximum rate of nuclear export achievable at saturation of endogenous carriers. The measured active-export time through the Nuclear Pore Complex (NPC) is 18 ms, remarkably similar to the previously determined active-import rate. Also, our results reveal that active export/import and active export/passive diffusion fluxes are uncoupled, thus complementing previous reports on active import/passive diffusion uncoupling. These findings suggest differential gating at the NPC level.**

The spatial separation of transcription and translation functions provides eukaryotes with powerful mechanisms to control gene expression, but demands finely tuned transport mechanisms between nucleus and cytoplasm to maintain the distinctive composition of each compartment. In this respect, the nuclear envelope (NE)[4] plays a crucial role since it is the barrier through which proteins and RNA must be transported in a regulated manner (1–3). The mediators of this exchange are nuclear pore complexes (NPCs). These comprise multiple copies of about 30 distinct proteins collectively called nucleoporins (4). Transport across the NPC was reviewed in detail (1–3, 5) and can be classified into two main modes. Small molecules such as ions, metabolites, and intermediate-sized macromolecules can freely diffuse through the NPC. This mechanism is increasingly restricted as the particle approaches a size limit of ~10 nm in diameter (6). Larger molecules such as proteins, RNAs, and their complexes are ushered selectively by dedicated transport receptors that can recognize specific nuclear localization (NLS) or nuclear export signal (NES) peptides displayed by the cargo itself (7). Several transport pathways exist, but most of them use a homologous family of carrier molecules collectively called karyopherins (8): import carriers are called importins and export carriers exportins. Most karyopherins bind directly to their cargoes; in some cases, however, karyopherins require adaptor proteins (9). Beside the cargo recognition sequence, karyopherins possess an NPC-binding domain and a binding domain for the GTPase Ran protein (9). Interaction with Ran is decisive for the directionality of active transport. In fact, association and dissociation of karyopherin-cargo complexes are regulated by binding to Ran in its two different forms: RanGTP and RanGDP. The interplay between a cytoplasmic RanGTPase activating protein (RanGAP), a nuclear Ran guanine nucleotide exchange factor (RanGEF, often referred to as RCC1), and a nuclear import factor for RanGDP establishes a Ran gradient across the NE, with high concentration of RanGTP in the nucleus and RanGDP in the cytoplasm. Importin-cargo affinity is strongly decreased by binding to RanGTP. Thus, importins bind to NLS-cargoes in the cytoplasm, where RanGTP is low, and release them in the nucleus upon binding with RanGTP. Conversely, RanGTP binding strongly favors NES-protein engagement by exportins in the nuclear compartment; cargoes are then released in the cytoplasm upon RanGAP-activated conversion of RanGTP to RanGDP (10).

Several classes of NLSs were identified (11, 12), but the leucine-rich (LR) NES is probably the better characterized to date. This sequence was first identified in HIV-1 Rev (13, 14) and is recognized by CRM1 (15). In this work, we select a prototypical NES sequence (LPPLERLTL) and address the thermodynamic details of its nucleocytoplasmic shuttling in live cells.

The ability to quantitatively study nucleocytoplasmic transport in live cells has been hindered by two main factors: the lack

* This work was supported in part by the Italian Ministry for University and Research (MIUR) under the framework of the FIRB Projects RBLA03ER38 and RBPR05JH2P, and PRIN 2008JZ4MLB.
[S] This article contains supplemental information with Equations S1–S10.
[1] Both authors contributed equally to this work.
[2] Present address: NKI The Netherlands Cancer Institute, Plesmanlaan 121 1066 CX, Amsterdam, The Netherlands.
[3] To whom correspondence should be addressed: Istituto di Biofisica-CNR, via Moruzzi 1-56124 Pisa, Italy. E-mail: r.bizzarri@sns.it.
[4] The abbreviations used are: NE, nuclear envelope; NES, nuclear export signal; NPC, nuclear pore complex; FRAP, fluorescent recovery after photobleaching; NLS, nuclear localization signal; FG-Nups, FG-nucleoporins.

of a method that can determine the active shuttling rates in single live cells and the inability to quantify the concentration of key molecular players at intracellular level. We recently tackled these issues by combining fluorescence recovery after photobleaching (FRAP) of GFP cargoes conjugated to transport sequences with the *in vivo* calibration of protein concentration. We obtained information on both thermodynamic (binding specificity and affinity) and dynamic (import rate) details of active import in intact cells (16, 17). In particular, in proliferating CHO-K1 cells we showed that a single NPC can support up to 90 NLS-mediated translocations/s from the cytoplasm to the nucleus. One must keep in mind that the same NPC must in parallel allow nucleus-to-cytoplasm export. Unfortunately, little knowledge of NES dynamics in intact cells is available, and the mutual influence between active export and passive diffusion is largely unknown. A recent report based on immunoelectron microscopy indicated that energy-dependent transport (import and export) and diffusion may take distinct spatial routes through the NPC (18). Similarly, Naim *et al.* (19) proposed that energy-dependent import and passive diffusion are not dynamically coupled.

In the present work, we tackle these issues by means of a FRAP-based strategy, using NES and NLS conjugated with optically distinguishable fluorescent proteins. More specifically we address the following questions: (*a*) what are the thermodynamic/kinetic details of nuclear export? (*b*) How do export parameters quantitatively compare with the corresponding nuclear import ones? (*c*) How do nuclear export and import compare in terms of fluxes? (*d*) Do nuclear import or passive diffusion modulate or interfere with nuclear export? We shall show that our data highlight the similarity between export and fluxes across the NPC, and their complete uncoupling. Also, we find that passive diffusion does not interfere with nuclear export, analogous to that reported by Naim *et al.* for nuclear import (19). We believe that these results can provide a useful reference framework for a thorough description of NPC.

## EXPERIMENTAL PROCEDURES

*Construction of Vectors*—Cloning of the NLS-Cherry construct used in this study was described in detail in a previous report (16). NES-EGFP plasmid was produced by two rounds of polymerase chain reaction (PCR) starting from EGFP template (pEGFP N1, Clontech, Mountain View, CA). Primers (all purchased by Sigma-Genosys) used in the first round were 5′-CTG GAA CGA CTG ACC CTG GAC GTG AGC AAG GTG AGC AAG GGC GAG-3′ and 5′-CCG GAA TTC CGG TTA CTT GTA CAG CAG CTC GTC CAT-3′. The forward primer consisted of two region, the first one contained the N-terminal region of NES, while the second one was partially matched with sequence encoding for N-term of EGFP; the reverse primer consisted of a region partially matched with sequence encoding for C-term of EGFP and another one containing the Eco*R*I site. In the second round the different forward primer 5′-CCC AAG CTT GGG ATG CTG CAG CTG CCA CCA CTG GAA CGA CTG ACC CTG GAC GTG-3′ was used, which consists of three regions containing respectively the HindIII site, the N-term region of NES and a sequence partially matching with the C-term NES portion added before. The resulting construct was inserted in the HindIII/EcoRI sites of pcDNA3.1(+) (Invitrogen).

*Cell Culture, Transfection, and Determination of the Global Protein Concentrations*—CHO K1 cells were acquired from the American Type Culture Collection (CCL-61 ATCC) and were grown in Ham's F12K medium supplemented with 10% fetal bovine serum, antibiotics (penicillin/streptomycin) at 37 °C and in 5% $CO_2$. The transfections of all constructs were carried out using Lipofectamine reagent (Invitrogen) according to manufacturer's instructions. For live imaging, 120000 cells were plated 24 h before transfection onto a 35-mm glass-bottom dish (WillCo-dish GWSt-3522). The global concentration of intracellular NES-EGFP- and of NLS-Cherry-linked proteins were determined by using the synthetic adduct fluorescein-glycine ("F-Gly") as described previously (16), and calibration was carried out separately for the two microscopes (see next section).

*Fluorescence Microscopy and Image Analysis*—Cell fluorescence was measured using two different microscopes, a Leica TCS SP2 inverted confocal microscope and Leica TCS SP5 inverted confocal microscope (Leica Microsystems AG, Wetzlar, Germany), both interfaced with an Ar laser for excitation at 458, 476, 488, and 514 nm, and with a HeNe laser for excitation at 543 and 633 nm. Glass-bottom Petri dishes containing transfected cells were mounted in a thermostated chamber (Leica Microsystems) and viewed with a 40 × 1.25-numerical aperture oil immersion objective (Leica Microsystems). Live cell imaging was always performed at 37 °C. Images were collected under 0.65–10 kW/cm$^2$ excitation power at the sample and monitoring the emission by means of the AOBS-based built-in detectors of the confocal microscopes. To increase the sensitivity the of Leica TCS SP2 microscope we used also APD (Avalance Photo Diode) detectors. The following collection ranges were adopted: 500–550 nm (GFP), 600–650 (Cherry). The background signal was subtracted from all images and data were analyzed using the ImageJ (NIH), version 1.42, and an implementation of the Igor-Pro software package.

*Fluorescence Recovery After Photobleaching: Experimental Details and Data Analysis*—Each FRAP experiment started with an eight-time line-averaged image (pre-bleach) of the cell followed by a single-point bleach (nonscanning) near the center of the nucleus with laser at full power (~50 kW/cm$^2$) for the minimum time required to photobleach most of nuclear fluorescence (3–4 s). Fluorescence recovery was measured by starting a time lapse acquisition within few milliseconds after bleaching. Image size was 512 × 512 pixels and scan speed was usually set to 800 Hz. Pinhole size was set to the optimal value of 1.0 Airy (corresponding to an 81.44 $\mu$m confocal aperture). Our model of nucleocytoplasmic exchange in the presence of both passive diffusion and active transport shows that the concentration of fluorescent species in the cytoplasm and nucleoplasm follows a first-order kinetics. Consequently the collected FRAP curves in both compartments were fitted to a single exponential (the fluorescence signal is assumed proportional to the concentration). Moreover, all images were normalized to the prebleaching signal to identify the presence of an immobile fraction.

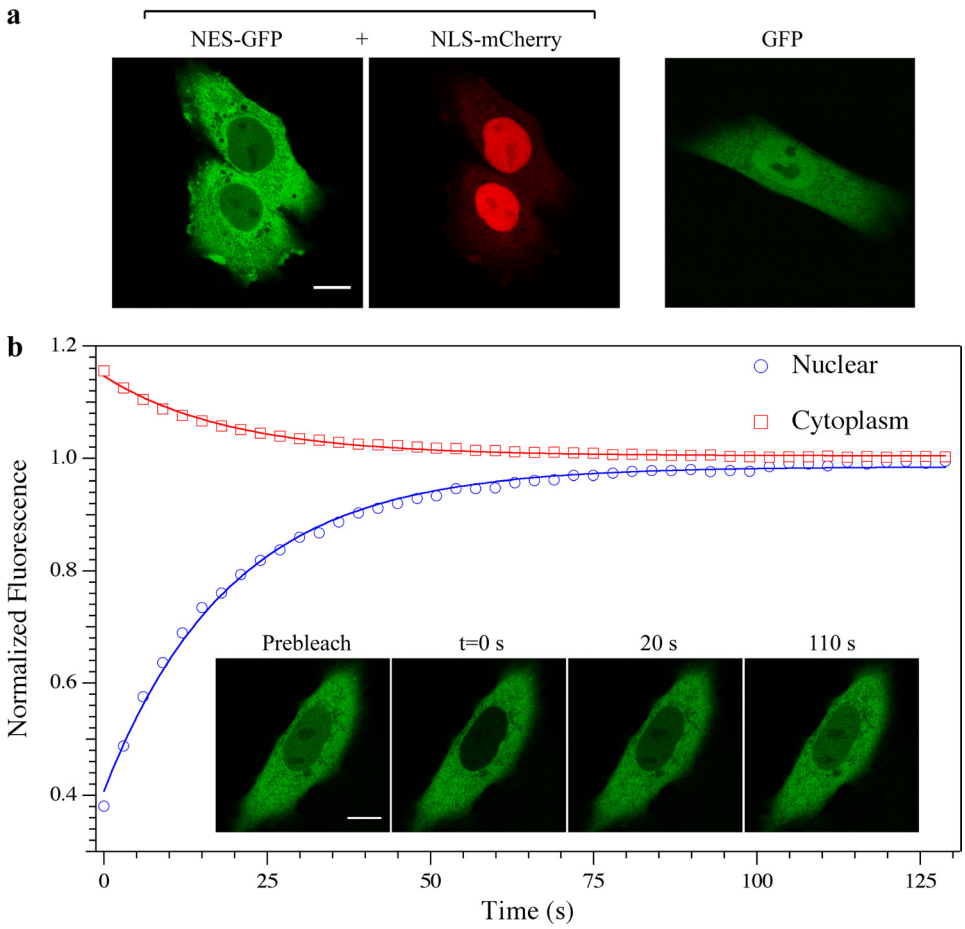


FIGURE 1. **Subcellular localization of protein constructs upon transfection and FRAP of NES-GFP.** *a*, cellular localization of NES-GFP, NLS-mCherry, and GFP analyzed by confocal imaging. Scale bars, 10 $\mu$m. *b*, FRAP analysis of NES-GFP. The plot reports the time-recovery of nuclear (*blue circles*) and cytoplasmic (*red squares*) fluorescence of NES-GFP following the photobleaching step; the continuous lines represent monoexponential fitting. Fluorescence confocal images of a cell undergoing FRAP are reported in the *inset* together with the acquisition time.

## RESULTS

*Subcellular Localization of NES-GFP and FRAP Analysis of Nucleocytoplasmic Shuttling*—The fluorescent fusion proteins used in this study were transiently expressed in live CHO-K1 cells and their subcellular localization analyzed by confocal microscopy (Fig. 1*a*). EGFP fused to NES (NES-GFP) is predominantly localized in the cytoplasm (Fig. 1*a*, *left panel*), consistently with the presence of the functional NES. As demonstrated in (16) and shown here for comparison, mCherry fused to the NLS of SV40 (hereafter denoted as NLS-mCherry) is significantly accumulated into the nucleus, whereas untagged GFP is homogeneously distributed across the NE (Fig. 1*a*, *center* and *right panels*). The balance between nuclear and cytoplasmic concentration can be quantitatively expressed by the parameter $K_{eq}$ defined as the ratio between nuclear and cytoplasmic concentration of the transported protein. It is apparent that $K_{eq} < 1$ for NES-GFP, $K_{eq} > 1$ for NLS-RFP, and $K_{eq} \sim 1$ for GFP.

*Kinetic Model of Nucleocytoplasmic Shuttling*—FRAP data were analyzed following a kinetic model of active/passive nucleocytoplasmic shuttling previously applied to nuclear import (16) and adapted to nuclear export (supplemental information). NES-GFP translocates across the NE according to two mechanisms: 1) passive diffusion from cytoplasm to nucleus (C→N) and vice-versa (N→C), on account of its molecular size below the exclusion value of NPC, 2) energy-dependent active export from nucleus to cytoplasm mediated by the exportin machinery (Scheme 1). Adapting Fick's 1st law to the passive transport we have Equations 1 and 2,

$$J_p^{C\to N} = P_{NES} \times C_{NES}^{C} \qquad \text{(Eq. 1)}$$

$$J_p^{N\to C} = P_{NES} \times \chi_{NES}^{N} \times C_{NES}^{N} \qquad \text{(Eq. 2)}$$

where $J_p^{C\to N}$ and $J_p^{N\to C}$ label passive-diffusion fluxes, $C_{NES}^{C}$ ($C_{NES}^{N}$) is the concentration of NES-GFP in the cytoplasm (nucleus), $\chi_{NES}^{N}$ labels the fraction of free NES-GFP (*i.e.* not bound to exportins) in the nucleus. The proportionality constant $P_{NES}$ is the permeability coefficient of the NE for free NES-GFP.

Two steps contribute to active nuclear export of NES-GFP (*a*) NES-GFP binding to exportin(s) (hereafter globally denoted by Ex) to form the NES-GFP$_n$·Ex complex (*n* represents the average number of NES-GFP molecules bound to each Ex molecule and plays the role of the Hill coefficient) in Reaction 1.

$$n\text{NES-GFP} + \text{Ex} \underset{}{\overset{K_D^*}{\rightleftharpoons}} \text{NES-GFP}_n\text{·Ex}$$

REACTION 1

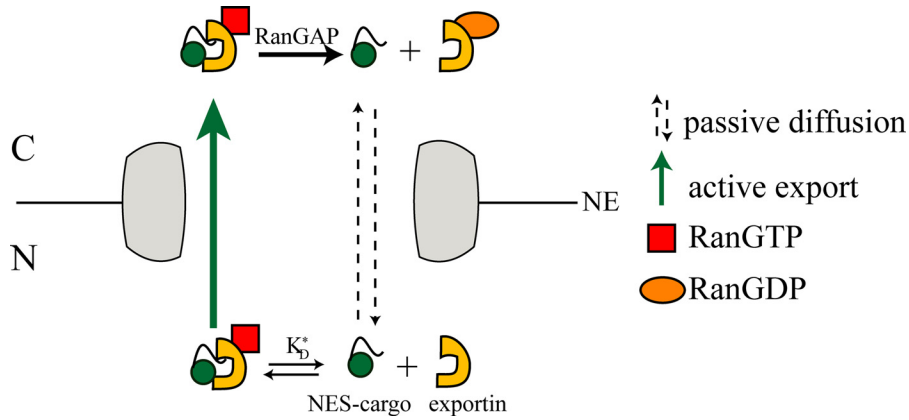


SCHEME 1. **Scheme of active and passive translocation of NES-GFP through the nuclear pore complex.**

$K_D^*$ is the intranuclear dissociation constant of the NES-$GFP_n$·Ex complex,[5] (*b*) active translocation of the NES-$GFP_n$·Ex complex from nucleus to cytoplasm. The resulting flux is proportional to the species nuclear concentration in Equation 3.

$$J_a^{N\to C} = \nu_{NES}^{N\to C}(1 - \chi_{NES}^{N})C_{NES}^{N} \qquad \text{(Eq. 3)}$$

$\nu_{NES}^{N\to C}$ ($\mu m^3/s$) can be considered as the "permeability coefficient" of active export. At saturating NES concentration, active flux reaches its maximum value (in the following: $V_m^{N\to C}$). $V_m^{N\to C}$ can be regarded as the intrinsic dynamic parameter characterizing nuclear export. It provides the maximum translocation capacity of the exportin machinery through the NPC in terms of exported molecules per second. Its reciprocal expresses the characteristic time required for a single NES-exportin complex molecule to cross the NPC.

FRAP is a relaxation technique that affects only the fluorescence of the protein label without perturbing the dynamic features of the protein of interest or its binding reactions. As a consequence we can assume that all intracellular processes occur at steady-state in the time course of FRAP experiments. For NES-GFP steady-state shuttling across NE implies[6] a constant ratio ($K_{eq}$) between $C_{NES}^{N}$ and $C_{NES}^{C}$ (note that both incorporate bleached and unbleached NES-GFP molecules and are not affected by the bleaching and following recovery). It is easy to demonstrate that both in the nucleoplasm and in the cytoplasm FRAP follows a first-order (*i.e.* monoexponential) time law (16) in Equation 4,

$$F_{C/N}(t) = F_{C/N}^{\infty} + (F_{C/N}^{0} - F_{C/N}^{\infty})\exp(-t/\tau) \qquad \text{(Eq. 4)}$$

where $\tau$ is the recovery time, C (N) labels cytoplasm (nucleus) quantities, and $F_{C/N}(t)$, $F_{C/N}^{0}$, and $F_{C/N}^{\infty}$, are the fluorescence intensity in the compartment of interest at time $t$, at time $t = 0$ (prebleach condition), and at long times when a new equilibrium between nucleus and cytoplasm is established, respectively. Once retrieved by fitting, the parameters in Equation 4 can be combined with the measured nuclear cell volume and $K_{eq}$ to recover $P_{NES}$ (16). Finally, the excess active flux of the exported protein $\phi^{N\to C}$ is obtained from Ref. 16 to give Equation 5.

$$\phi^{N\to C} = P_{NES}\left(\frac{1}{K_{eq}} - 1\right)C_{NES}^{N} \qquad \text{(Eq. 5)}$$

$\phi^{N\to C}$ is an experimentally measurable parameter, and it corresponds to the global N→C flux (passive+active) minus the theoretical passive N→C flux of NES-GFP in absence of exportin. Specifically to what we have demonstrated for the active nuclear import of NLS-GFP (16), the experimental plot of $\phi^{N\to C}$ *versus* $C_{NES}^{N}$ must contain all the relevant features of active NES export from nucleus. $\phi^{N\to C}$ grows linearly with $C_{NES}^{N}$ until a significant fraction of NES is engaged in the complex with exportin, then it levels off. The asymptotic $\phi^{N\to C}$ value is $V_m^{N\to C}$, and the shape of the curve may lead to $K_D^*$ determination once the stoichiometry of the complex is known. The supplemental information reports Equations S8–S10 relating $\phi^{N\to C}$ with $C_{NES}^{N}$ for a 1:1 complex, since the putative exportin for NES (CRM1) contains a single binding site for leucine-rich sequences (15). In the following sections we shall discuss experimental values of $V_m^{N\to C}$, $K_D^*$, and $P_{NES}$ as calculated from FRAP data according to this theoretical framework.

*Analysis of NES-GFP Active Nuclear Export*—FRAP was first applied to analyze the nucleocytoplasmic shuttling of NES-GFP in cells expressing this protein alone. The nuclear fluorescence of NES-GFP was photobleached, and the subsequent recovery was monitored by time-lapse imaging (Fig. 1*b*, *inset*). The fluorescence recovery in the nucleoplasm (or the decay in the cytoplasm) was well fitted by monoexponential equations, consistently with the kinetic behavior of our model of nucleocytoplasmic exchange (Fig. 1*b*).

Actual $C_{NES}^{N}$ values were determined from the prebleach fluorescence intensity of the nucleus with a calibration based on F-Gly (16).

Fig. 2*a* shows $\phi^{N\to C}$ *versus* $C_{NES}^{N}$. Notably, experimental values of $C_{NES}^{N}$ span a wide range because of the large expression variability of the NES-GFP cargo and so do excess active export flux values. $\phi^{N\to C}$ increases almost linearly with concentration up to $C_{NES}^{N} \sim 10\ \mu M$ and then levels off. This indicates that up to this concentration the endogenous export system is operating below maximum capacity.

Fitting $\phi^{N\to C}$ *versus* $C_{NES}^{N}$ data with supplemental Eqs. S8 and S10 yields $K_D^* = 15 \pm 7\ \mu M$ and $V_m^{N\to C} = 1.1 \pm 0.3{\cdot}10^5$ molecule/s. Assuming $2{\cdot}10^3$ NPCs per nucleus (21), this value translates into about 56 molecule/s per single NPC, *i.e.* a char-

[5] The asterisk indicates that the dissociation constant is in principle different from the actual *in vitro* binding constant, because of the intranuclear environment: see next sections for further details on this point.

[6] From the steady state condition $J_p^{C\to N} + J_p^{N\to C} + J_a^{N\to C} = 0$.

acteristic translocation time of about 18 ms for each NES molecule.

Available *in vitro* assays showed that the thermodynamic dissociation constant of NES·CRM1 complex ($K_D$) is somewhat lower than $K_D^*$, its effective value in the nucleus ($K_D$ ranges from 0.5 to 7 $\mu$M, (22, 23)). We previously stressed that $K_D^*$ can be higher than $K_D$, on account of the presence in the nucleus of competitors and spatially heterogeneous binding phenomena (16). Remarkably, the calculated $K_D^*$ is very close to that displayed by the NLS-Importin complex (16 ± 7 $\mu$M). This indicates that import and export machineries operate by engaging cargo molecules in complexes of analogous thermodynamic stability. The intracellular environment, however, seems to affect much less NES-GFP binding to CRM1 ($K_D^*/K_D = 2 \div 30$) than NLS-GFP binding to Importin-$\alpha$ ($K_D^*/K_D \sim 400$).

*Analysis of NES-GFP Active Nuclear Export in the Presence of NLS-Cherry*—In order to assess whether active nuclear import interferes in any way with active nuclear export, we performed FRAP measurements on NES-GFP in cells co-expressing NLS-mCherry. This additional label made it possible to quantify NLS concentration before the bleaching step. In view of maximizing a possible coupling/interfering effect, we restricted our analysis to cells expressing high concentration of NES-GFP and NLS-mCherry. This ensures that both export and import cellular machinery operate at cargo saturating levels. Despite the high activation of nuclear import, the retrieved $\phi^{N\to C}$ values of NES-GFP were totally consistent with those obtained in absence of NLS-mCherry at the same $C^N_{NES}$ (Fig. 2*a*, *crossed squares*). The lack of any coupling mechanism between active nuclear export and import is suggested by the highly random scatter of $\phi^{N\to C}$ *versus* $C^C_{NLS}$ (Fig. 2*b*, *crossed squares*).

*Analysis of NES-GFP Passive Nucleocytoplasmic Shuttling in the Absence or in Presence of NLS-Cherry*—Fig. 2*c* reports the $P_{NES}$ *versus* $C^N_{NES}$ plot in absence and in presence of NLS-Cherry. The clear independence of $P_{NES}$ in the range of explored $C^N_{NES}$ indicates that the NE permeability to passive diffusion of NES-GFP is independent from NES-GFP or NLS-Cherry concentration. This implies that active export and passive transport are negligibly coupled in cells, consistently with the analogous behavior described for NLS-cargoes (19). Notably, the average value $\bar{P}_{NES} = 9.5 \pm 5\ \mu m^3/s$ is comparable to the average permeability coefficient obtained for GFP alone ($\bar{P}_{GFP} = 13 \pm 4\ \mu m^3/s$) and NLS-GFP, $\bar{P}_{NLS} = 5.4 \pm 3\ \mu m^3/s$). This is not surprising since passive translocation of both NES-GFP and NLS-GFP is dominated by the size of the GFP unit, on account of the much smaller size of the NES and NLS stretches.

## DISCUSSION

The NES-GFP chimera was transfected in live cells and its intracellular transport quantitatively analyzed by means of a FRAP-based approach recently developed in the context of NLS-driven active transport (16, 17). Thanks to this method we can estimate both NES affinity for its nuclear export carrier(s) (Ex, in the present case CRM1) and NE permeability to active export. The former is quantified by $K_D^*$, the dissociation constant of the NES-GFP·Ex complex in the nucleus, the latter by the maximum flux rate $V^{N\to C}_m$. $V^{N\to C}_m$ corresponds to the rate of active N→C translocation of NES-GFP engaged in binding

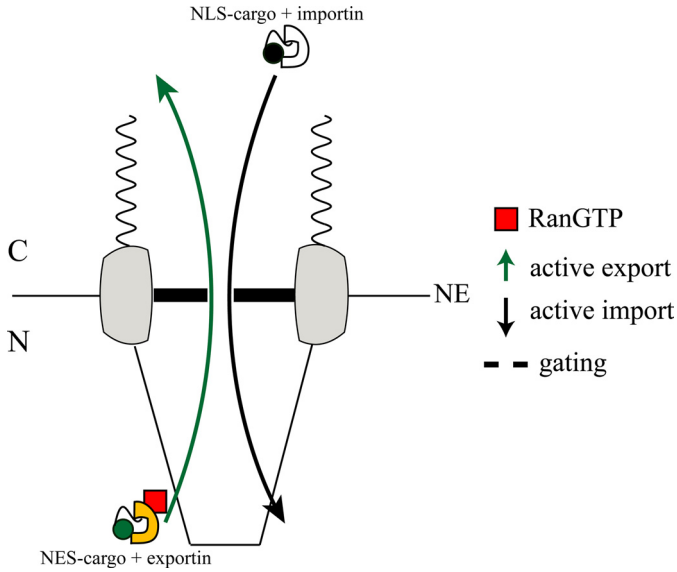


SCHEME 2. **Pictorial description of NPC gating activity with respect to active nuclear export and import.**

exportin. Because of its independence from the exportin concentration $V^{N\to C}_m$ can well describe the intrinsic dynamical properties of the export machinery.

The first result of the present work is that $V^{N\to C}_m = 1.1 \pm 0.3 \cdot 10^5$ molecule/s, a value comparable to that obtained in (16) for the nuclear import of NLS-GFP, or NLS-$GFP_2$: $V^{C\to N}_m = 1.8 \pm 0.1 \cdot 10^5$ molecule/s. This shows a remarkable similarity between the two translocation machineries. When $V^{N\to C}_m$ and $V^{C\to N}_m$ are translated into the average time required for each translocation event, both export (18 ms) and import (11 ms) values are in agreement with single molecule correlation measurements performed on NLS-GFP either on an ensemble of pores (24) or at the single-pore level (25). These data are also in agreement with the C→N flux of the import complex calculated at physiological importin concentration by Ribbeck *et al.* (21).

These findings can provide useful indications on the regulation of molecular transport across the NE. The fact that despite their structural difference importin and exportin complexes exhibit similar values of translocation efficiency suggests that the dynamic characteristics of NE crossing stem largely from the "gating" properties of NPC (Scheme 2). This in turn can help identify the nature of the mechanism governing the pore function. In recent years much debate has taken place on the mechanical basis of translocation through the NPC (5). Some authors proposed that the FG-nucleoporins (FG-Nups) inside the pore undergo gel-liquid transition to allow the passage of the transport complex (26, 27); other authors suggested a mechanical collapse of the same FG-Nups upon transport-complex binding (28); a further description invokes the sliding of transport receptors over freely moving FGNups filaments (2). Our findings indicate that the correct molecular description must take into account the comparable translocation efficiency values of structurally different importin and exportin complexes.

The present work shows also that active import and export processes are uncoupled transport processes, and the same

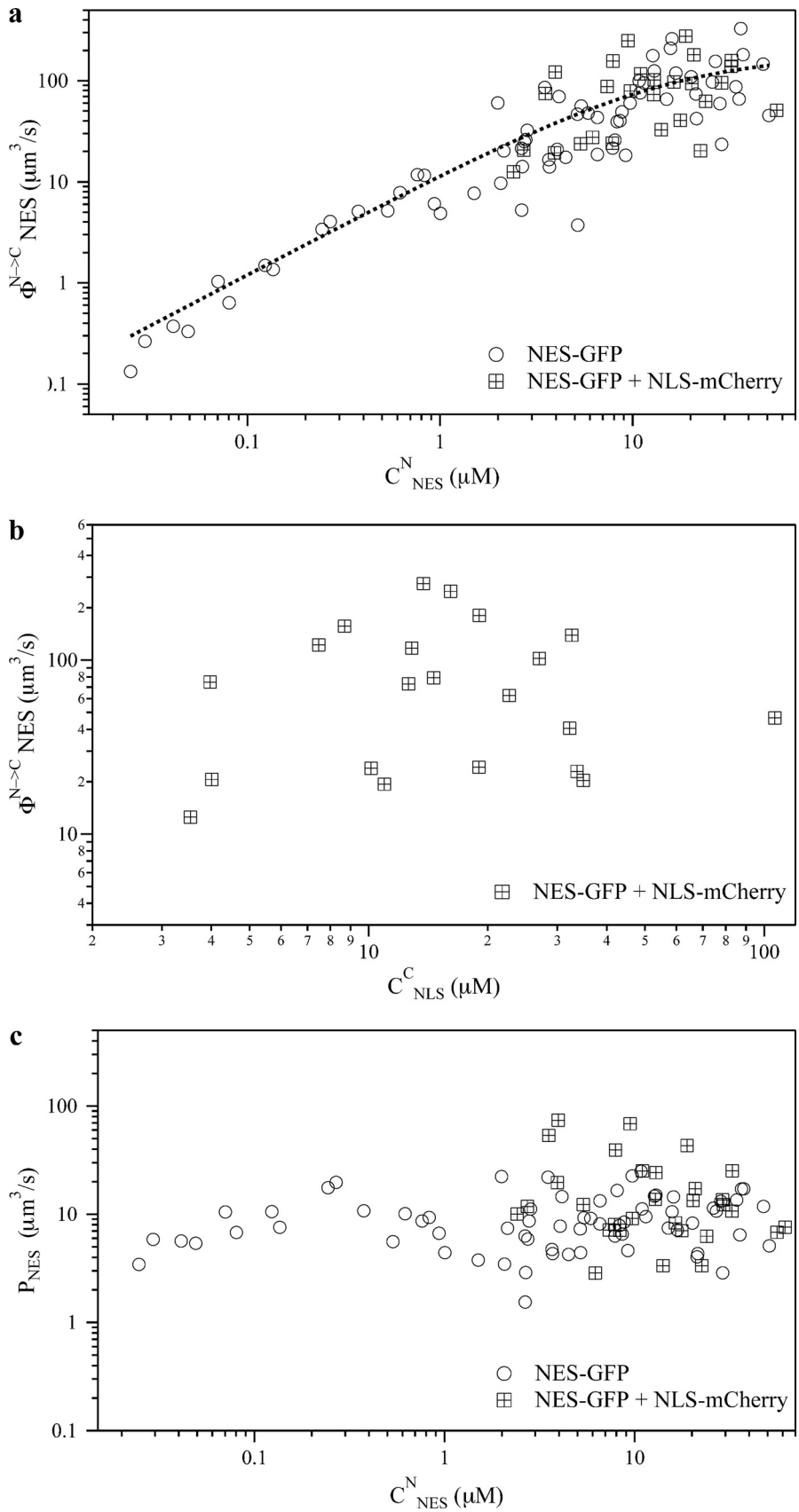


FIGURE 2. **Dynamic properties of NES-GFP nucleocytoplasmic translocation in absence (*circles*) or presence (*crossed squares*) of NLS-mCherry.** *a*, plot of the FRAP-recovered active excess flux of NES-GFP *versus* nuclear NES-GFP concentration; fit of experimental data to Eqs. S8–S10 is reported by a *dashed line*. *b*, plot of the FRAP-recovered active excess flux of NES-GFP *versus* cytoplasm concentration of co-expressed NLS-mCherry. *c*, plot of the FRAP-recovered NE passive permeability of NES-GFP *versus* nuclear NES-GFP concentration.

applies to active export and passive diffusion. This can be inferred from the negligible dependence of the kinetic parameters on the concentration of expressed NES-GFP or NLS-GFP (Fig. 2, *a* and *b*), and the close similarity of the NE passive permeability of NES-GFP, NLS-GFP, and GFP regardless of cargo concentration (Fig. 2*c*). This uncoupling of the translocation mechanisms is strongly suggestive of a structural separation of these processes within the NPC, as recently proposed by others (18, 19). Alternatively, in fact, one would have to require the fine tuning of the thermodynamic characteristics of active and passive fluxes inside the same NPC channel to prevent interference and allow their separate modulation.

Finally, we determined an estimate of the dissociation constant between NES-GFP and the exportin receptor, *i.e.* CRM1. When $K_D^*$ is compared with the intrinsic $K_D$ measured i*n vitro*, we find that the intracellular environment lowers the binding affinity by 0.5–2 kcal/mol of free energy at 37 °C.[7] Interestingly, we previously reported a larger reduction of binding affinity for the NLS-GFP/Importin-$\alpha$ couple at intracellular level compared with *in vitro* condition (3.7 kcal/mol, (16)). This suggests that active transport across the NE is not only related to the gating properties of NPC but also to the modulation of molecular recognition between the cargo and its transporter protein. Several intracellular factors may contribute to this affinity modulation including: (i) competition of endogenous NES-like sequences with expressed NES-GFP for CRM1 binding; (ii) spatial heterogeneity of CRM1 concentration in the nucleus (also suggested in Refs. 23, 29) that was not taken into account in the FRAP analysis; (iii) nonspecific interactions of the NES sequence with intra-nuclear moieties. Concerning this last effect, a similar modulation was observed in the cytoplasm for the binding of Tat peptide and derived mutants with importins (30).

These dynamical properties are not specific to the particular cargo considered here but are relevant to other NES-cargo complexes. Indeed, at exportin (or importin) saturation our approach yields the intrinsic translocation properties of the export (import) complex through NPC. This is clearly shown by the fact that the same translocation efficiency was obtained for NLS conjugated to one or two GFP molecules (16).

Care must be taken when discussing the modulation of cargo binding affinity. Although we showed that NLS-GFP and NLS-$GFP_2$ bind with the same strength to the importin complex, we should not exclude the influence of cargo structure on $K_D^*$ for both nuclear export and import. Also, we focused on the Rev-derived NES stretch that is known to interact with CRM1; other NES interacting with other exportins are likely to be characterized by different $K_D^*$ values. Further experiments need to be carried out to elucidate this point and to assess whether the observed symmetric behavior of nuclear export and import extends also to the cargo-binding step, as suggested by the close $K_D^*$ values of NES-GFP and NLS-GFP or NLS-$GFP_2$.

In conclusion, FRAP-based experiments allowed us to probe the major dynamic features of NES active transport across the NE. We showed that active export and import are uncoupled transport processes and they take place with similar timing at NPC level. Uncoupling extends also to active and passive transport processes. These findings suggest differential gating properties at the level of the individual nuclear pore. A further way to modulate fluxes resides in the fine-tuning of cargo-transporter binding affinity. We believe these results can stimulate further studies on nucleocytoplasmic transport mechanisms at molecular level by means of FRAP and other techniques.

[7] The change in free energy of binding is calculated as $\Delta G = +RT\ln(K_D^*/K_D)$.

## REFERENCES


1. Görlich, D., and Kutay, U. (1999) Transport between the cell nucleus and the cytoplasm. *Annu. Rev. Cell Dev. Biol.* **15,** 607–660
2. Macara, I. G. (2001) Transport into and out of the nucleus. *Microbiol Mol. Biol. Rev.* **65,** 570–594
3. Weis, K. (2003) Regulating access to the genome: nucleocytoplasmic transport throughout the cell cycle. *Cell* **112,** 441–451
4. Cronshaw, J. M., Krutchinsky, A. N., Zhang, W., Chait, B. T., and Matunis, M. J. (2002) Proteomic analysis of the mammalian nuclear pore complex. *J. Cell Biol.* **158,** 915–927
5. Fahrenkrog, B., and Aebi, U. (2003) The nuclear pore complex: nucleocytoplasmic transport and beyond. *Nat. Rev. Mol. Cell Biol.* **4,** 757–766
6. Paine, P. L. (1975) Nucleocytoplasmic movement of fluorescent tracers microinjected into living salivary gland cells. *J. Cell Biol.* **66,** 652–657
7. Pemberton, L. F., and Paschal, B. M. (2005) Mechanisms of receptor-mediated nuclear import and nuclear export. *Traffic* **6,** 187–198
8. Conti, E., Müller, C. W., and Stewart, M. (2006) Karyopherin flexibility in nucleocytoplasmic transport. *Curr. Opin. Struct. Biol.* **16,** 237–244
9. Wente, S. R., and Rout, M. P. (2010) The nuclear pore complex and nuclear transport. *Cold Spring Harb. Perspect. Biol.* **2,** a000562
10. Walde, S., and Kehlenbach, R. H. (2010) The part and the whole: functions of nucleoporins in nucleocytoplasmic transport. *Trends Cell Biol.* **20,** 461–469
11. Dingwall, C., Sharnick, S. V., and Laskey, R. A. (1982) A polypeptide domain that specifies migration of nucleoplasmin into the nucleus. *Cell* **30,** 449–458
12. Kalderon, D., Roberts, B. L., Richardson, W. D., and Smith, A. E. (1984) A short amino acid sequence able to specify nuclear location. *Cell* **39,** 499–509
13. Fischer, U., Huber, J., Boelens, W. C., Mattaj, I. W., and Lührmann, R. (1995) The HIV-1 Rev activation domain is a nuclear export signal that accesses an export pathway used by specific cellular RNAs. *Cell* **82,** 475–483
14. Neville, M., Stutz, F., Lee, L., Davis, L. I., and Rosbash, M. (1997) The importin-beta family member Crm1p bridges the interaction between Rev and the nuclear pore complex during nuclear export. *Curr. Biol.* **7,** 767–775
15. Dong, X., Biswas, A., Süel, K. E., Jackson, L. K., Martinez, R., Gu, H., and Chook, Y. M. (2009) Structural basis for leucine-rich nuclear export signal recognition by CRM1. *Nature* **458,** 1136–1141
16. Cardarelli, F., Bizzarri, R., Serresi, M., Albertazzi, L., and Beltram, F. (2009) Probing nuclear localization signal-importin $\alpha$ binding equilibria in living cells. *J. Biol. Chem.* **284,** 36638–36646
17. Cardarelli, F., Serresi, M., Albanese, A., Bizzarri, R., and Beltram, F. (2011) Quantitative analysis of Tat peptide binding to import carriers reveals unconventional nuclear transport properties. *J. Biol. Chem.* **286,** 12292–12299
18. Fiserova, J., Richards, S. A., Wente, S. R., and Goldberg, M. W. (2010) Facilitated transport and diffusion take distinct spatial routes through the nuclear pore complex. *J. Cell Sci.* **123,** 2773–2780
19. Naim, B., Brumfeld, V., Kapon, R., Kiss, V., Nevo, R., and Reich, Z. (2007) Passive and facilitated transport in nuclear pore complexes is largely uncoupled. *J. Biol. Chem.* **282,** 3881–3888
20. Deleted in proof
21. Ribbeck, K., and Görlich, D. (2001) Kinetic analysis of translocation through nuclear pore complexes. *EMBO J.* **20,** 1320–1330
22. Paraskeva, E., Izaurralde, E., Bischoff, F. R., Huber, J., Kutay, U., Hartmann, E., Lührmann, R., and Görlich, D. (1999) CRM1-mediated recycling of

snurportin 1 to the cytoplasm. *J. Cell Biol.* **145,** 255–264
23. Lindsay, M. E., Holaska, J. M., Welch, K., Paschal, B. M., and Macara, I. G. (2001) Ran-binding protein 3 is a cofactor for Crm1-mediated nuclear protein export. *J. Cell Biol.* **153,** 1391–1402
24. Cardarelli, F., and Gratton, E. (2010) In vivo imaging of single-molecule translocation through nuclear pore complexes by pair correlation functions. *PLoS One* **5,** e10475
25. Cardarelli, F., Lanzano, L., and Gratton, E. (2011) Fluorescence correlation spectroscopy of intact nuclear pore complexes. *Biophys. J.* **101,** L27–29
26. Ribbeck, K., and Görlich, D. (2002) The permeability barrier of nuclear pore complexes appears to operate via hydrophobic exclusion. *EMBO J.* **21,** 2664–2671
27. Frey, S., Richter, R. P., and Görlich, D. (2006) FG-rich repeats of nuclear pore proteins form a three-dimensional meshwork with hydrogel-like properties. *Science* **314,** 815–817
28. Lim, R. Y., Fahrenkrog, B., Köser, J., Schwarz-Herion, K., Deng, J., and Aebi, U. (2007) Nanomechanical basis of selective gating by the nuclear pore complex. *Science* **318,** 640–643
29. Daelemans, D., Costes, S. V., Lockett, S., and Pavlakis, G. N. (2005) Kinetic and molecular analysis of nuclear export factor CRM1 association with its cargo *in vivo*. *Mol. Cell Biol.* **25,** 728–739
30. Cardarelli, F., Serresi, M., Bizzarri, R., and Beltram, F. (2008) Tuning the transport properties of HIV-1 Tat arginine-rich motif in living cells. *Traffic* **9,** 528–539